

**Technical Advice and Support for the  
Cargo Advanced Automated Radiography System (CAARS)  
Program**

**Task 2.2 Transmission Digital Radiography (DR)**

Final Report

DNDO Program Manager: Dr. Joel Rynes

Cary Pincus, Dr. Diane Chinn, Dr. Harry Martz,  
John Rodriguez, Randall Thompson

Principal Investigator: Dr. Harry Martz [martz2@llnl.gov](mailto:martz2@llnl.gov)

Project Engineer: Buzz Pedrotti [pedrotti1@llnl.gov](mailto:pedrotti1@llnl.gov)

Lawrence Livermore National Laboratory  
Livermore, CA 94551

Work performed on the  
Domestic Nuclear Detection Office (DNDO) of the  
Department of Homeland Security  
Statement of Work: IAA No. HSHQDC-08-X-00388  
Some of this work was also performed under the DNDO Joint Integrated  
Non-Intrusive Inspection (JINII) program.

27 June 11

LLNL-TR-473131-Final



 **Lawrence Livermore  
National Laboratory**



This document was prepared as an account of work sponsored by an agency of the United States government. Neither the United States government nor Lawrence Livermore National Security, LLC, nor any of their employees makes any warranty, expressed or implied, or assumes any legal liability or responsibility for the accuracy, completeness, or usefulness of any information, apparatus, product, or process disclosed, or represents that its use would not infringe privately owned rights. Reference herein to any specific commercial product, process, or service by trade name, trademark, manufacturer, or otherwise does not necessarily constitute or imply its endorsement, recommendation, or favoring by the United States government or Lawrence Livermore National Security, LLC. The views and opinions of authors expressed herein do not necessarily state or reflect those of the United States government or Lawrence Livermore National Security, LLC, and shall not be used for advertising or product endorsement purposes.

This work performed under the auspices of the U.S. Department of Energy by Lawrence Livermore National Laboratory under Contract DE-AC52-07NA27344.

# 1. Executive Summary

The Cargo Advanced Automated Radiography System (CAARS) program<sup>1</sup> aims to utilize advanced radiographic systems to detect radiological and nuclear threats. Validation of initial design and testing concepts is a precondition for prototype system development and large-scale deployment. As expected, Depleted Uranium (DU) is a valid surrogate for Special Nuclear Materials (SNM) in CAARS Advanced Technology Demonstration (ATD) performance field-tests of transmission radiography systems. Dual-energy transmission measurements of DU are nearly identical to SNM, and are distinct from lower Z materials, provided the samples are matched to equal areal density. Results from an alternative method, using samples of equal thickness, showed sample discrimination by material density, rather than by atomic number (Z). The transmission measurements of DU and SNM were made with equipment that is nearly identical to current field systems.

X-ray source beams at endpoint energies of 5.4 MeV and 9.6 MeV were used to measure transmission through the selected sample materials. The ratio of the x-ray linear attenuation coefficient times length ( $\mu L$ ) at 5.4 MeV, to  $\mu L$  at 9.6 MeV is a metric for atomic number based discrimination of materials. The measured ratios were compared

<b>Table 1.</b> Ratio of material $\mu L$ values of 5.4 and 9.6 MeV endpoint energy Linatron source beams, measured and computed, for samples with areal density of 73.4 g/cm <sup>2</sup>			
Material	Measured Ratio	Computed Ratio	Z
WGPu	1.059 +/- 0.005	1.080	94
HEU	1.062 +/- 0.004	1.080	92
DU	1.059 +/- 0.005	1.081	92
Pb	1.060 +/- 0.005	1.079	82
W	1.062 +/- 0.005	1.081	74
Sn	1.097 +/- 0.006	1.112	50
Fe	1.183 +/- 0.008	1.187	26

with computed values based on LLNL photon cross section data<sup>2</sup> and LLNL developed models of x-ray detector characteristics<sup>3</sup>. Measured ratios for DU differed from HEU by an average of 0.25%, and from WGPu by 0.08%, which is within the noise level of 0.4 to 0.5%. For comparison, measured ratios for Sn differed from HEU by 3.2%, and from

<sup>1</sup> Work was also performed under the Joint Integrated Non-Intrusive Inspection (JINII) program

<sup>2</sup> D.E. Cullen, M.H. Chen, J.H. Hubbell, S.T. Perkins, E.F. Plechaty, J.A. Rathkopf, J.H. Scofield, "Tables and Graphs of Photon-Interaction Cross Sections from 10 eV to 100 GeV Derived from the LLNL Evaluated Photon data Library (EPDL)", UCRL-50400, Vol. 6, Part A, Rev. 4, October 31, 1989

<sup>3</sup> A. E. Schach von Wittenau, C. M. Logan, M. B. Aufderheide and D. M. Slone, "Blurring artifacts in megavoltage radiography with a flat-panel imaging system: Comparison of Monte Carlo simulations with measurements", Med. Phys. 29 (11), Nov. 2002, pp. 2559-2570

WGPu by 3.6%, well beyond the measurement noise. Measured ratios for W differed from HEU by 0.01%, and from WGPu by 0.32%.

The measured ratio values presented in Table 1 demonstrate the feasibility of using a threshold ratio to discriminate low- $Z$  ( $Z < 72$ ) from high- $Z$  ( $Z \geq 72$ ) materials (as defined by CAARS specification). In the case of our test system, a threshold ratio of 1.08 would be suitable based on the measured results.

## 2. Introduction

### 2.1 *Program Overview*

Covert nuclear attack is one of the foremost threats facing the United States and is a primary focus of the War on Terror. The Domestic Nuclear Detection Office (DNDO), within the Department of Homeland Security (DHS), is chartered to develop and improve domestic systems to detect and interdict smuggling for the illicit use of a nuclear explosive device, fissile material or radiological material.

The CAARS ATD program<sup>1</sup> is a major part of the DHS effort to enhance US security by harnessing cutting-edge technologies to detect radiological and nuclear threats at points of entry to the United States. DNDO has selected vendors to develop complete radiographic systems. It is crucial that the initial design and testing concepts for the systems be validated and compared prior to the substantial efforts required to build and deploy prototypes and subsequent large-scale production.

Lawrence Livermore National Laboratory (LLNL) is funded by DHS to provide a variety of services including radiological and nuclear physics, engineering and radiography. LLNL is a primary resource for subject matter experts in nuclear and radiological detection systems and radiography. LLNL provides Science and Technical Advisory Support to DNDO, performing five tasks related to the independent evaluation of CAARS vendor systems. The five tasks are:

- Task 1: Scientific and technical advice and consultation
- Task 2: DU and Special Nuclear Material (SNM) experiments
- Task 3: Performance assessment simulations of vendor systems
- Task 4: Threat matrix simulations of vendor systems
- Task 5: Validate Surrogate Test Matrix

The tasks performed take advantage of unique capabilities and facilities at LLNL. Substantial expertise in radiography, extensive computational resources, advanced physics (Monte Carlo) and engineering (straight ray) X-ray radiography simulation codes and a Category 3 Nuclear (X-ray facility that can handle SNM) Facility at LLNL are used to support this project.

### 2.2 *Purpose*

The purpose of Task 2.2 (Transmission DR measurements) is to demonstrate the suitability of using Depleted Uranium (DU) as a valid surrogate for SNM in CAARS ATD performance tests of transmission and radiography systems. The CAARS transmission radiography systems use megavolt (MeV) Bremsstrahlung photon beam sources to irradiate the cargo. The CAARS systems perform Atomic Number (Z) discrimination by analyzing results of interactions that are dependent on the Z of the material comprising the cargo. These interactions are not isotopically sensitive. That is, they are not Mass Number (A) dependent. Therefore, one should not draw the conclusion that if DU is a good surrogate for transmission radiography, DU would provide a suitable test surrogate for isotopically sensitive discrimination techniques (e.g., Nuclear Resonance Fluorescence).

DU is considered as a surrogate because its Z is similar to the Z of SNM materials. In addition, fabrication of surrogate objects is facilitated by commercially available sources for DU stock. DU also offers relatively simple handling, tracking and transport requirements compared to SNM. If DU is proven to be a suitable surrogate, multiple test objects can be designed, manufactured and distributed to test vendor systems.

### **2.3 Objectives**

The primary Transmission DR test activity objective reflects the dual-energy approach used by the CAARS contractors:

- Compare dual-energy, single-aspect transmission radiography signatures of DU, HEU, and Weapons Grade Plutonium (WGPu) to determine if DU is a suitable test surrogate for HEU and WGPu to support CAARS ATD testing.

In addition, there are two secondary Transmission DR test activity objectives that provide additional baseline information to support CAARS ATD testing:

- Record transmission signatures of non-SNM materials that may be effective in shielding SNM. The materials included in this test are lead, tungsten, tin and steel.
- Study the variation in responses from different detectors in transmission. One detector studied may be used in CAARS ATD testing – a Varian 9 MeV energy matched linear detector array substantially identical to the L3 CAARS ATD system.

### **2.4 Physical Basis**

Transmission of the x-rays through the samples is modeled and measured for two source endpoint energies. The transmission values will differ for each material due to the distinct mass absorption characteristics of each material at each of the energies. We make use of the fact that the energy dependence of the mass absorption differs for materials with different atomic numbers.

Appendix B contains charts showing the photon cross sections of the sample materials over the 1 to 10 MeV energy range. Additionally, the cross sections for six component interactions are shown. For example, at 5 MeV the mass absorption coefficient of tungsten has roughly equal contributions from incoherent (Compton) scatter and pair-production. This energy is a cross-over point between these two contributing factors which dominate the total attenuation cross section over our energy range. Also, near the cross-over point the total mass absorption is near a local minimum. At energies lower than the cross-over point the mass absorption is dominated by Compton scatter, at higher energies it is dominated by pair-production.

Low Z elements have mass absorption coefficient curves that intersect within the lower energy regime. This results in similar integrated transmission values for the 5.4 MeV endpoint energy. The low Z elements have mass absorption coefficient values that diverge in the higher energy regime. The attenuation values go down with decreasing atomic number. The ratio of the results

for 5.4 MeV to the results for 9.6 MeV increase with decreasing atomic number for the lower  $Z$  samples.

In contrast, the higher atomic number elements, in terms of mass absorption relative to each other, behave much the same whether one considers an incident x-ray spectrum from a 5.4 MeV endpoint source, or from the source with a 9.6 MeV endpoint energy. Accordingly, the ratio of the results for 5.4 MeV to the results for 9.6 MeV maintain a consistent relationship for the higher  $Z$  samples. Thus the measured ratio shows  $Z$  dependence for low  $Z$  materials and relatively little  $Z$  dependence for high  $Z$  materials.

### **3. Test Approach**

#### ***3.1 General Test Plan***

LLNL performed experiments to compare measured transmission of an x-ray source with nominal endpoint energies of 5 MeV and 9 MeV through three nuclear materials and four metals: U238 (DU), U235 (highly enriched uranium – HEU), Weapons Grade Pu239 (WGPu), lead, tungsten, tin and steel. Transmission studies of standardized samples allowed comparison of the properties of each material under similar high-energy x-ray interrogation methods being developed by CAARS vendors. Appendix A contains a detailed description of the test plan and methodology.

#### ***3.2 Test Timetable***

Milestones for this project were:

- Fabrication of samples complete – August, 2010
- Measurements complete – November, 2010
- Detector studies complete – November, 2010

## 4. Test Objects

### 4.1 *Material Constraints*

Special nuclear material control at LLNL is governed by DOE order M470.4-6, “Nuclear Material Control and Accountability”. To minimize the amount of security oversight required by this DOE order, we performed experiments using Graded Safeguard Category III quantities of SNM. This limits the amount of SNM in the facility to the following quantities at one time.

- WGPu - 400 grams
- HEU – 1 kg
- DU – no limit

Operations in LLNL’s high-energy radiography facility must comply with LLNL document FSP-239-09, “Weapons and Complex Integration Directorate Radiography Facility Building 239 Facility Safety Plan (FSP)”. Controls for Radioactive Material in the FSP include a requirement for containment of SNM at all times when the material is in the facility. Containment must consist of single containment with a welded metal barrier or double containment with at least one barrier being a sealed, rigid-walled metal container. To minimize container costs, we use double containment of SNM.

### 4.2 *Material Sample Matrix*

The sample matrix is designed to simulate a cube of DU with a nominal volume of  $100 \text{ cm}^3$ . To take advantage of existing LLNL SNM manufacturing capabilities, the test is performed using cylindrical specimens. The nominal DU cube dimension ( $100^{1/3} = 4.64 \text{ cm}$ ) is used as the length of the WGPu cylinder. The diameter of the WGPu cylinder, 2.6 cm, is chosen to ensure that a single WGPu specimen does not exceed the 400 gram Category III limit on individual WGPu parts.

Two samples sets are fabricated, each set containing the three nuclear materials and four metals. Both sets have the same diameter, 2.6 cm, as the WGPu. The lengths of the two sets differ. Sample set 1 has specimen cylinder lengths chosen such that the product of the density times length ( $\rho L$ , or areal density) is equal for all specimens in the set. Sample set 2 specimens are machined to a cylinder length of 4.64 cm to match the nominal length of the WGPu samples.

The actual measured density and chemical composition for each specimen in Sample set 1 was used to calculate exact lengths. Lengths of Sample set 1 specimens range from approximately 4.0 cm to 13 cm. In Sample Set 1, two or three specimens of each material are manufactured for statistical purposes. Sample Set 2 has one specimen of each material. All specimens are machined to a tolerance of  $\pm 0.025 \text{ cm}$  in length and diameter. Table 2 shows the lengths of each of the specimens in the sample matrix.

In the manufacturing of the three WGPu samples, two of the samples (Pu2 & Pu3) were produced with densities in the expected range, and one was measured to have a higher density (Pu1). The two in-range samples (Pu2 & Pu3) were machined to a length of 4.64 cm, and a target areal density ( $\rho L$ ) of 73.4 g/cm<sup>2</sup> was calculated based on the average  $\rho L$  of Pu2 and Pu3. Sample Pu1 was then machined to a shorter length to have the same value of  $\rho L$ .

The lengths, L, of the other samples were calculated based on measured density values of the rough cut stock prior to final machining.

$$\begin{aligned} \rho_{\text{WGPu}} &= 15.81 \text{ g/cm}^3 \\ \rho_{\text{DU}} &= 19.00 \text{ g/cm}^3 \\ \rho_{\text{HEU}} &= 18.63 \text{ g/cm}^3 \\ \rho_{\text{Pb}} &= 11.33 \text{ g/cm}^3 \\ \rho_{\text{W}} &= 19.16 \text{ g/cm}^3 \\ \rho_{\text{Sn}} &= 7.29 \text{ g/cm}^3 \\ \rho_{\text{Fe}} &= 7.83 \text{ g/cm}^3 \end{aligned}$$

Sample Set	WGPu Length (cm)	HEU Length (cm)	DU Length (cm)	Pb Length (cm)	W Length (cm)	Sn Length (cm)	Fe Length (cm)
1-1	4.47	3.94	3.88	6.50	3.83	10.06	9.36
1-2	4.64	3.94	3.87	6.50	3.83	10.06	9.37
1-3	4.64		3.88	6.49	3.84	10.06	9.37
2	4.64	4.64	4.66	4.65	4.64	4.64	4.64

**Table 2.** Sample matrix. All samples are cylinders, 2.6 cm dia.

Transmission measurements acquire data for either constant areal density (Set A) or constant length (Set B1 and B2). Table 3 shows the three transmission data sets. Set A and Set B1 transmission measurements are made along the axial path through the Sample set 1 and Sample set 2 cylinders, respectively. Set B2 represents transmission measurements made along a radial path, normal to the axis of the sample cylinders, with a path length of 2.6 cm, and includes both Sample set 1 and Sample set 2.

Data Set	Sample Set	Sample Constraint	X-Ray Transmission Direction
A	1	Areal Density . $\rho L = 73.4 \text{ g/cm}^2$	Axial
B1	2	Length . $L = 4.64 \text{ cm}$	Axial
B2	1 & 2	Length . $L = 2.6 \text{ cm}$	Radial

**Table 3.** Three transmission data sets each include 7 materials (3 nuclear materials and 4 metals).

### 4.3 Transmission Modeling and Measurement

Measured x-ray transmission includes source photon flux density, transmission through intervening matter (primarily the sample item) and detector response. We compare our measurements with predicted values based on modeled spectra of the x-ray beam, convolved with models for the energy deposition characteristics of each detector system.

For a given element, the photon flux density is calculated by:

$$\Phi = \Phi_0 [S(E)] e^{-\mu(E,Z)\rho L}$$

where

$\Phi_0$  = incident photon flux density

$\Phi$  = emerging flux density

S = Source spectrum

E = Energy

$\mu(E,Z)$  = mass absorption coefficient (Z and energy dependent)

Z = material atomic number

$\rho$  = material density

L = material thickness

Theoretical x-ray attenuation is determined by integrating the x-ray source energy spectrum transmitted through the sample, given the total x-ray photon cross-section as a function of energy. One approach to the experiment design is to calculate the transmission for the WGPu samples, and determine the length of each other sample material necessary to produce the same transmission for the selected x-ray source spectrum. However, the resulting sample lengths will not perform in measurements exactly as modeled, due to compromises in the models for the source spectrum, photon interactions and detector response. Also, if one were to design samples that were matched for one endpoint-energy spectrum, they will have different attenuations for the other endpoint energy, and additional transmission variations when a different detector system is utilized. That is, a null result experiment for one source endpoint energy would be difficult to achieve, and is not necessary to accomplish the goals of this task.

The approach that we implemented for transmission Set A was to equilibrate the product of density and length ( $\rho L$ , or areal density) for the samples. For samples with equal values of  $\rho L$ , differences in transmission are a function of the mass absorption (itself a function of atomic cross-section and incident photon energy). It is then relatively straightforward to both model and measure the ability of a source-detector system to discriminate between Set A samples based on x-ray transmission. Note that because the Set A samples have the same value of  $\rho L$ , as well as the same cylinder diameter, their masses will be equal.

Transmission of the x-rays through the samples is modeled and measured for two source endpoint energies. The transmission values will differ for each material due to the distinct mass absorption characteristics of each material at each of the energies. We make use of the fact that the energy dependence of the mass absorption differs for materials with different atomic numbers.

The nominal low energy setting of our Varian M9 dual energy Linatron source is 5 MeV but has been calculated, based on factory testing, to have an endpoint energy of 5.4 MeV. The nominal high energy setting of the source is 9 MeV but was calculated to have an endpoint energy of 9.6 MeV.

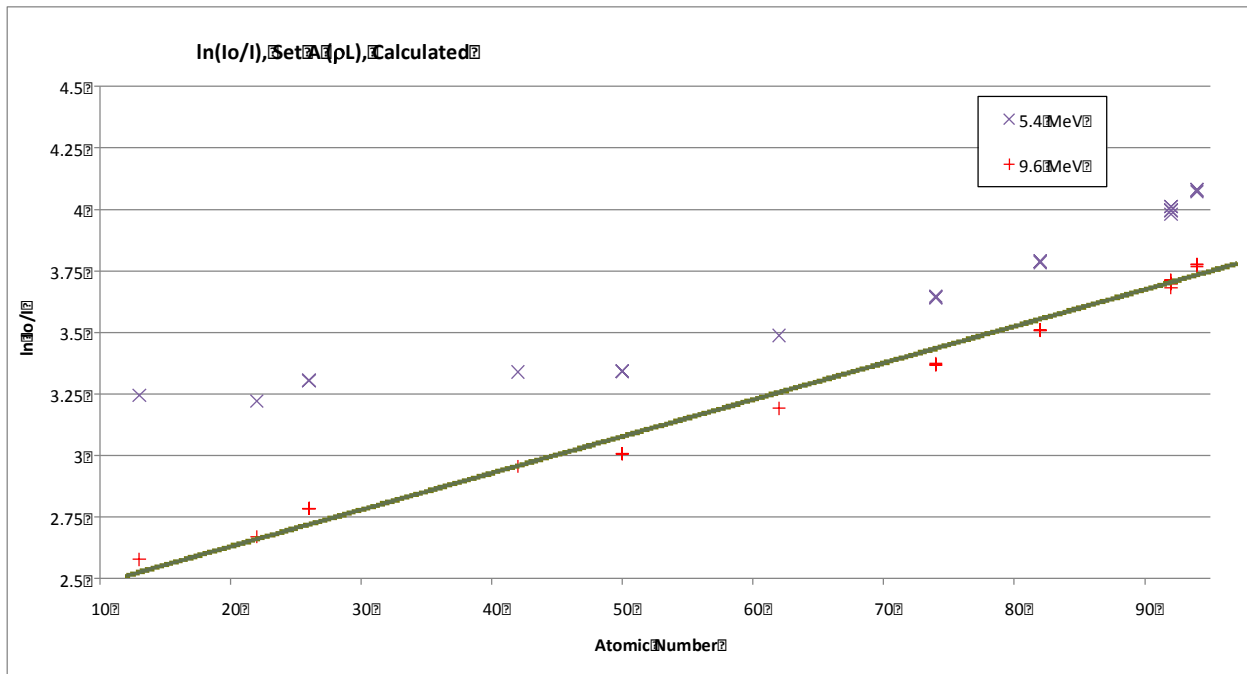


**Figure 1.** Calculated values of  $\ln(I_o/I)$  for Set A samples in our modeled source-detector system, at source energies of 5.4 and 9.6 MeV. Additional virtual samples (Al, Ti, Mo and Sm) are included to emphasize the trend for each energy.

The product of linear attenuation and length is mathematically equivalent to the natural log of the ratio of the incident flux ( $I_o$ ) to the transmitted flux ( $I$ ). Calculated values of  $\ln(I_o/I)$  for Set A samples are shown in Figure 1. The calculations are derived from LLNL tables photon cross sections (Cullen, *et al.* 1989) combined with modeled spectra for the Varian Linatron source and linear detector array. Values are plotted for low and high (5.4 and 9.6 MeV) endpoint energies.

The values for the high energy spectra are fairly linear, whereas the trend for the low energy spectra has a knee. Accordingly, the ratios of the low to high energy values are relatively constant in the high  $Z$  regime ( $Z \geq 72$ ), and diverge from each other in the low  $Z$  regime.

Appendix B contains charts showing the photon cross sections of the sample materials over the 1 to 10 MeV energy range. Additionally, the cross sections for the six component interactions are shown. For example, at 5 MeV the mass absorption coefficient of tungsten has roughly equal contributions from incoherent (Compton) scatter and pair-production. This energy is a cross-over point between these two contributing factors which dominate the total attenuation cross section over our energy range. Also, near the cross-over point the total mass absorption is near a local minimum. At energies lower than the cross-over point the mass absorption is dominated by Compton scatter, at higher energies it is dominated by pair-production.

For elements of lower atomic number than tungsten, such as tin and iron, the cross-over point occurs at higher energies, 6.4 MeV for tin and 9.6 MeV for iron. Conversely, for elements of higher atomic number than tungsten, such as lead, uranium and plutonium, the cross-over point occurs at lower energies, 4.8 MeV for lead, 4.4 MeV for uranium and 4.4 MeV for plutonium. The total cross sections for our sample materials, shown in Appendix B, are converted to mass absorption coefficients and combined into a single plot for comparison in Figure 2.

Figure 2 shows the mass absorption coefficient for the sample materials over the energy range relevant for the measurements. Aluminum is included for illustrative purposes. The curves for the higher atomic number elements, tungsten, lead, uranium and plutonium, are similar to each other, with primarily a change in magnitude. The lighter elements, tin, iron and aluminum, follow different trajectories, in accordance with the higher photon energies required for pair production to occur in the vicinity of lower mass nuclei.

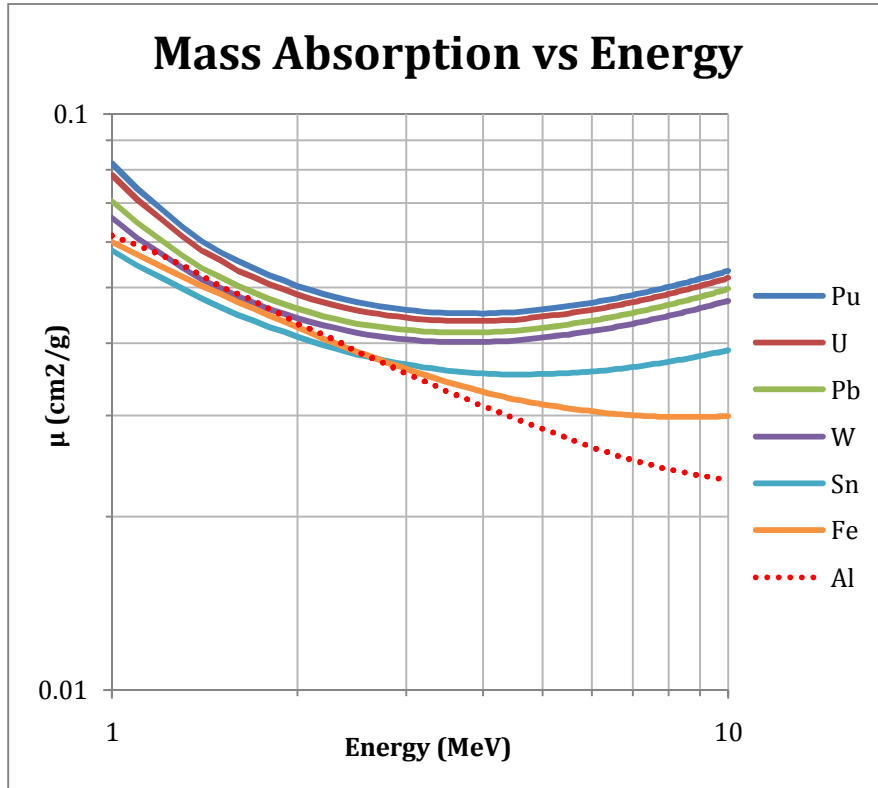


**Figure 2.** Mass absorption coefficients of selected elements, versus incident photon energy

The lighter elements have mass absorption coefficient values that intersect within the lower energy regime. This results in similar transmission values for the 5.4 MeV endpoint energy. The lighter elements have mass absorption coefficient values that diverge in the higher energy regime. The attenuation values go down with decreasing atomic number. The ratio of the results for 5.4 MeV to the results for 9.6 MeV increase with decreasing atomic number for the lower Z samples.

In contrast, the higher atomic number elements, in terms of mass absorption relative to each other, behave much the same whether one considers an incident x-ray spectrum from a 5.4 MeV endpoint source, or from the source with a 9.6 MeV endpoint energy. Accordingly, the ratio of transmission measurements for 5.4 MeV to the results for 9.6 MeV maintain a consistent relationship for the higher Z samples.

Figure 3 shows a comparison of the combined spectral characteristics of two source-detector pairings. The detector spectra were calculated using a Monte Carlo N-Particle (MCNP) transport code<sup>4</sup>. The thicker detector elements of the linear detector array result in a greater number of secondary interactions contributing to the measured signal. As photon energies increase there is increased energy deposited in the linear detector array crystals.

<sup>4</sup> MCNP: A General Monte Carlo N-Particle Transport Code, Version 5, Volume I: Overview and Theory, X-5 Monte Carlo Team, Los Alamos National Laboratory report LA-UR-03-1987, April 24, 2003.

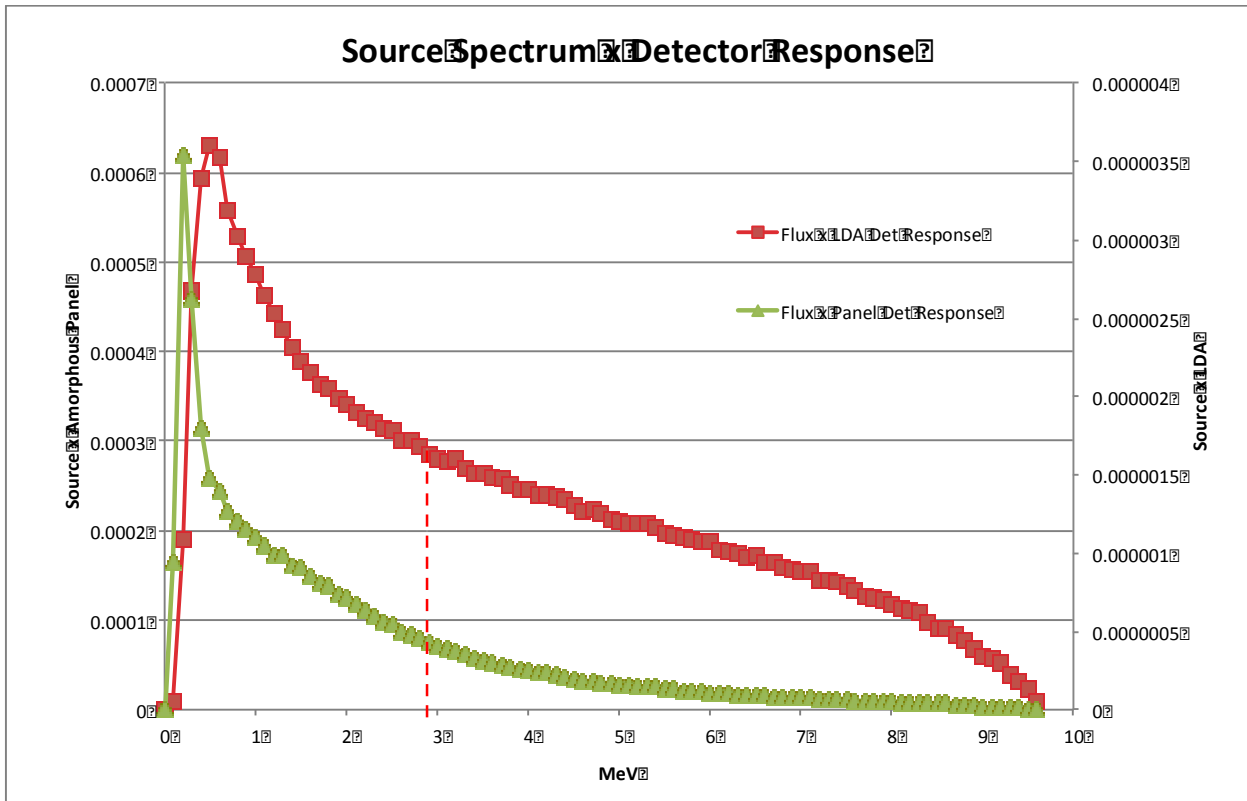


**Figure 3.** The product of the source spectrum (9.6 MeV endpoint energy) and detector spectral response, versus incident photon energy, for the 2D amorphous panel detector (green) and the linear detector array (red).

By integrating under the curves for the source set to 9.6 MeV we arrive at mean energies of 1.3 MeV for the amorphous panel and 2.9 MeV for the linear detector array.

Transmission measurements were modeled with HADES, an x-ray ray-tracing code developed at LLNL<sup>5,6</sup>. The HADES predicted results matched transmission results calculated using LLNL table mass absorption by the samples, and MCNP derived energy deposition in the LDA detector elements.

<sup>5</sup> M. B. Aufderheide, D. M. Slone, A. E. Schach von Wittenau, "HADES, A Radiographic Simulation Code", in *Review of Progress in Quantitative Nondestructive Evaluation*, **20A**, 2000, D. Thompson and D. Chimenti, eds., AIP Conf. Proc. 557, pp. 507-513.

<sup>6</sup> M.B. Aufderheide, G. Henderson, A.E. Schach von Wittenau, D.M. Slone, H.E Martz, "HADES, a code for simulating a variety of radiographic techniques", in *2004 IEEE Nuclear Science Symposium Conference Record*, Volume 4, pp. 2579 - 2583, Digital Object Identifier 10.1109/NSSMIC.2004.1462780

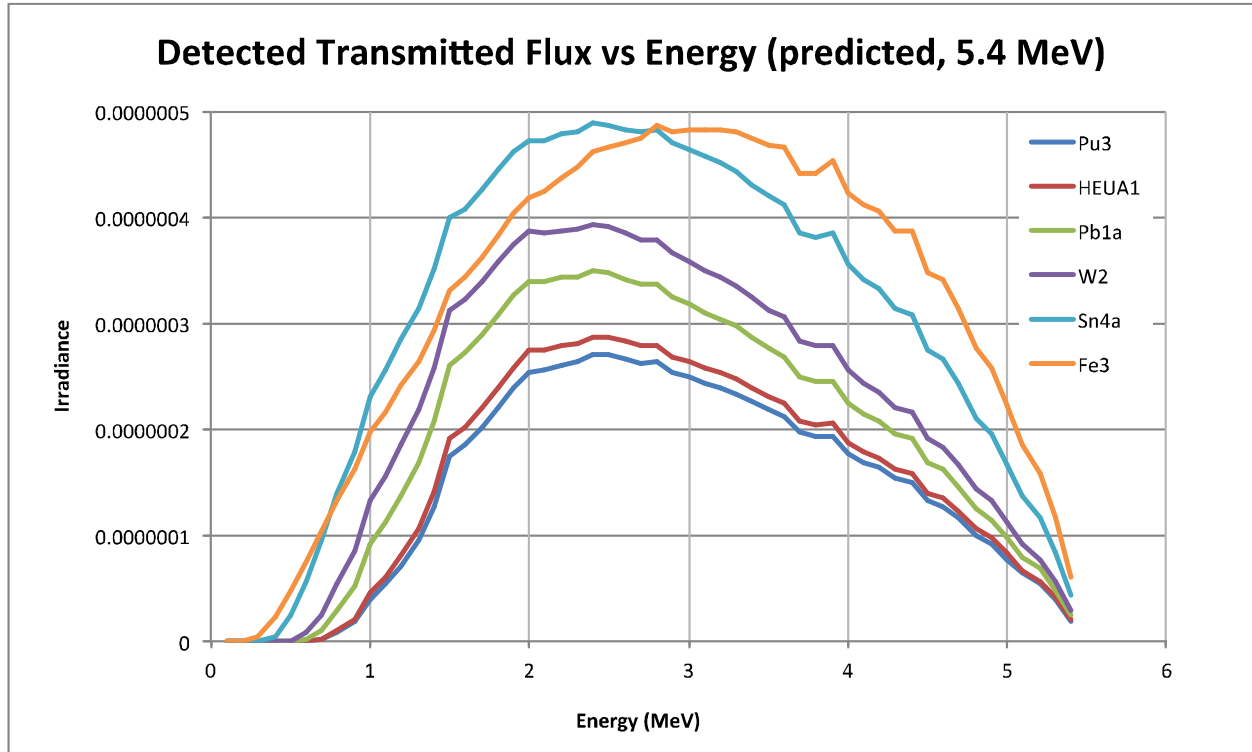


**Figure 4.** Detected, transmitted flux of selected elements, versus incident photon energy

Figure 4 shows curves for predicted results of transmission measurements for representative Set A examples of the sample matrix and the 5.4 MeV endpoint energy. The transmitted irradiance is the product of the source spectra, the transmission through the sample, and the detector response in each energy interval. The total measured transmission corresponds to the integration of the areas below the curves. The areas beneath the curves for Sn4a and Fe3 are roughly equal, therefore the modeled transmission values for the two samples are the same for the 5.4 MeV endpoint energy setting.

The contrast in behavior for the lighter elements Fe and Sn can be seen in the difference in relative areas under the curves, as shown in Figures 4 and 5.

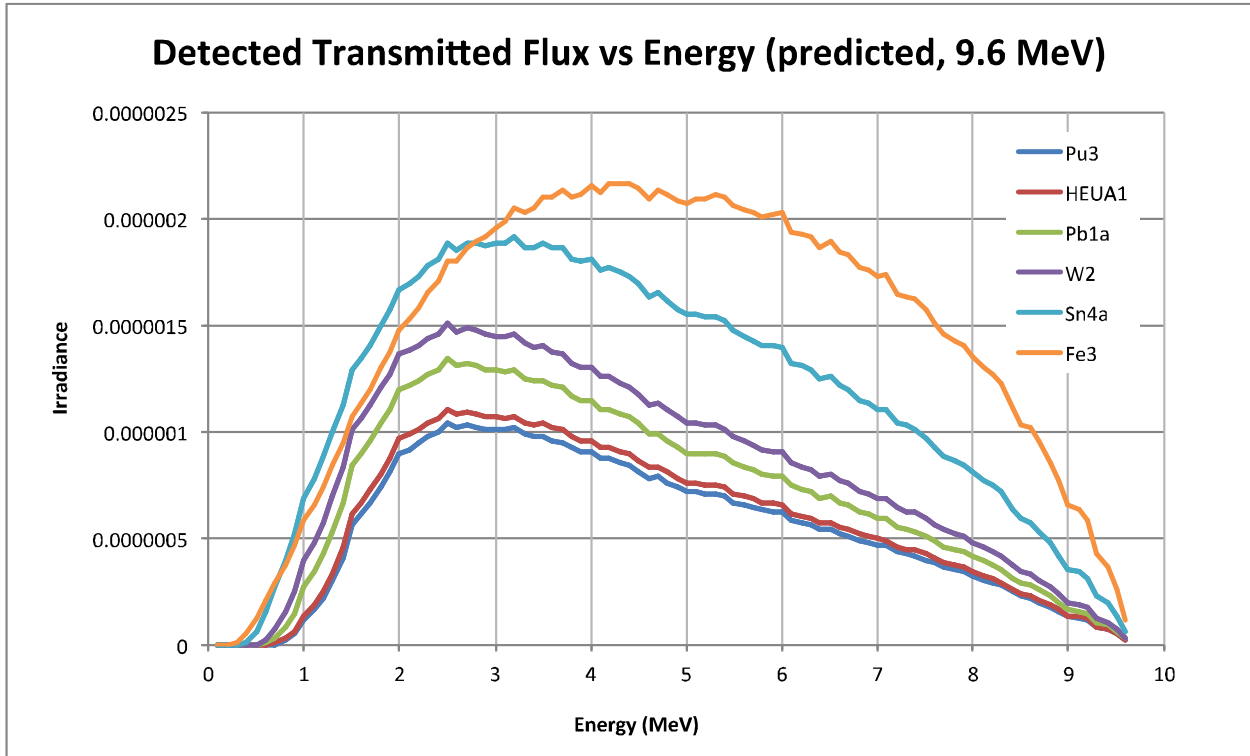


**Figure 5.** Detected, transmitted flux of selected elements, versus incident photon energy

Figure 5 shows curves for predicted results of transmission measurements for representative Set A examples of our sample matrix and the 9.6 MeV endpoint energy. The area beneath the curve for Fe3 is larger than the area for Sn4a. Iron is predicted to allow greater transmission of the higher energy source than tin samples of equal  $\rho L$ .

Taking the ratio of the calculated integrated transmissions for sample Fe3 at the two energies (5.4 to 9.6 MeV), and comparing it with the ratio calculated for sample Sn4a, one would expect from the values shown in Figures 4 and 5 that the ratio would be lower for Fe3 (because of the relatively larger transmission in the denominator). Likewise there is a difference in calculated ratios for sample Sn4a versus sample W2, but the differences in the areas under the curves are less visually obvious.

The areas under the curves for the high Z materials remain in constant proportion, and accordingly the ratios are very close in value. Ratios of attenuation follow the same pattern, except that for the low Z materials the ratio increases with decreasing Z. The values shown in Table 1 illustrate the consistent attenuation ratio for the high Z materials and the diverging attenuation ratios for the lighter elements tin and iron. Thus there is a basis for discrimination between the Set A materials utilizing the x-ray transmission measured at the two energies.

Because Set B samples are equivalent in length, the density of the samples can become an overriding factor. For instance, tungsten at atomic number 74 and lead at atomic number 82 have relatively similar mass absorption coefficients, compared to their relative densities, as tungsten is roughly 1.7 times higher. Equivalent length samples of the two materials will have

distinct transmission values largely determined by the density difference, which can overshadow the relatively smaller differences due to their atomic numbers. Additionally, larger differences in raw transmission mean that the “hardness” of the x-ray beam will vary more widely over the range of Set B samples than the Set A samples.

#### **4.4 Packaging**

Because of facility constraints, each sample was packaged individually. Packaging was identical for all samples to ensure that the only difference between the samples is due to the difference in materials. Samples were placed in a crossed plate aluminum holder, then sealed in a polyvinyl chloride bag, approximately 0.33-mm thick. The sample and bag were placed in a sealed steel paint can, approximately 0.23-mm thick, which is approved for transport of SNM. The can has an inner diameter of 164 mm, inside height of 178 mm and a volume of 3.76 L. The holder was designed to have “transmission windows” through the holder both longitudinally and laterally, for axial and radial measurements of the samples, respectively. Foam rubber spacers, placed at the top and bottom of the paint can, keep the holder in position inside the can. The position of the holder relative to the can was marked on the outside of the can. A sketch and a photograph of the can configuration are shown in Figure 6.

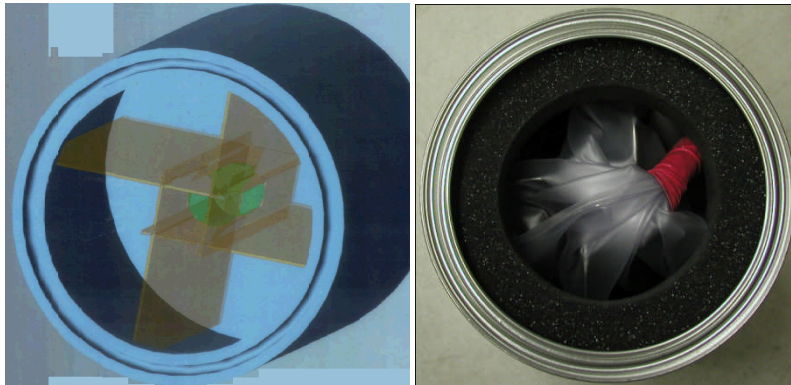


**Figure 6.** Sketch and photograph of package containing sample and holder inside can.

## **5. Test Configurations**

### **5.1 Transmission Measurement Equipment**

Transmission measurements were acquired using a Varian M9 dual-energy Linatron at 5 MeV and 9 MeV nominal endpoint energies. Two detector systems were employed. The first was a Thales amorphous silicon ( $\alpha$ -Si) panel detector. The second was a Varian Linear Detector Array (LDA).

The sample paint cans were placed at the front of the x-ray source and measured one at a time. Additionally, the characteristics and size of the LDA allowed us to place two paint cans, side by side, at a distance halfway between the source and detector. Measurements were made with samples oriented so that the direction of beam travel is either in line with the cylindrical axis (0

degrees, at left in figures) or perpendicular to the cylindrical axis (90 degrees, at right in figures), as shown in Figures 7 and 8.

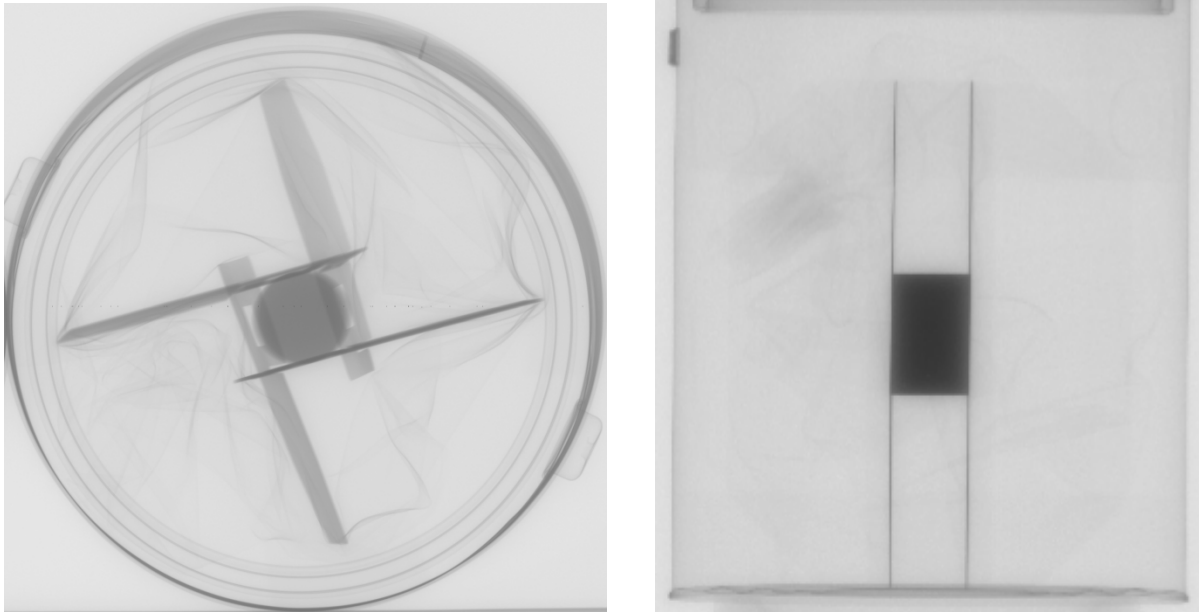


**Figure 7.** Axial (“0 degrees”, left) and radial (“90 degrees”, right) radiographs of samples in paint cans. Direction of beam travel is normal to image plane. Images produced with sample cans near amorphous silicon panel detector.

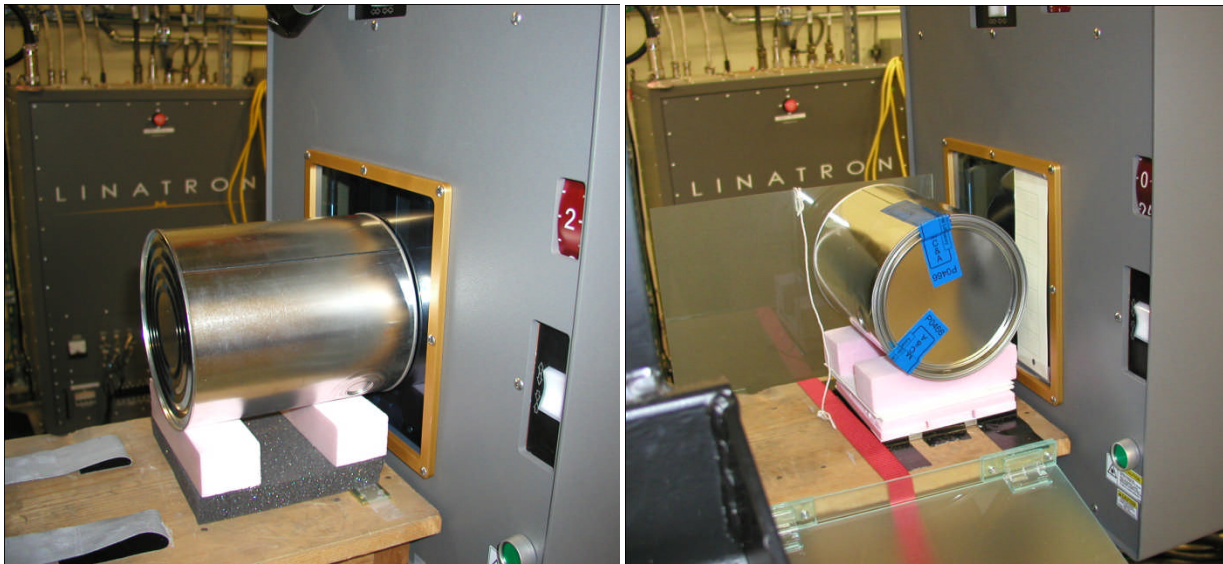


**Figure 8.** Paint cans positioned close to x-ray source for axial (left) and radial (right) measurement of samples.

## 5.2 *Transmission Measurement Procedures*

The data acquisition procedures are listed in Appendix A.

## 6. Results

### 6.1 *Overview of the Measurements*

The measurements of transmission were made with the expectation that the behavior would follow the predictions produced by the models. The CAARS ATD systems utilize a dual energy measurement approach that should be able to distinguish between high  $Z$  ( $\geq 74$ ) and low  $Z$  ( $< 74$ ) materials. The transmission measurements were used to calculate a ratio value for each material sample that corresponds to the relative attenuation by the low-energy x-ray versus high-energy x-ray beams.

The attenuation of the samples was such that there was a great deal of attenuation of the x-ray beams, leaving only a small amount of signal relative to the sources of noise. The amorphous panel detector, having a relatively thin profile in the direction of the x-ray beam, was particularly susceptible to errors and inconsistencies in comparison with modeled results. This is most likely due to a sharp falloff in its response to higher energy photons.

The linear detector array, which was designed for use with high energy x-ray sources, had much higher signal to noise characteristics, and the measured results were much closer to model predictions. For our sample set, a threshold value for the measured ratio can be used to distinguish between high and low  $Z$  materials.

### 6.2 *Panel Detector Measurements*

The measurements of the samples with the amorphous panel detector are shown on the following figures. The measured results show the ratio values of the samples:

$$\ln(I_0/I)@5.4 \text{ MeV} / \ln(I_0/I)@9.6 \text{ MeV}$$

Error bars have not yet been calculated for the amorphous panel measurements.

Figure 9 (below) shows the ratio values of the Set A data samples, measured with the axis of the samples aligned with the x-ray beam (axial, or 0 degree). There is some evidence of clustering of the values for the higher Z elements. The measurements of the lower Z elements are more chaotic. It would be difficult to set a threshold value for the ratio based on the data acquired.

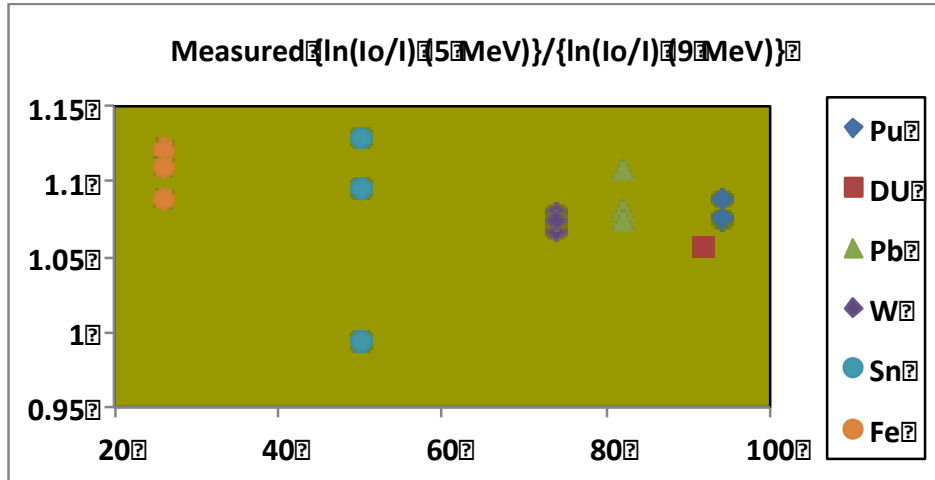


Figure 9. Measurements of ratio values for the Set A data samples, measured axially.

Figure 10 (below) shows the predicted ratio values of the Set A data samples, measured with the axis of the samples aligned with the x-ray beam (axial, or 0 degree). One could set a threshold value for the ratio at approximately 1.16 based on the predicted results. However, the data acquired would indicate a different value for the threshold, and the failure of the results to behave as modeled would render any threshold meaningless.

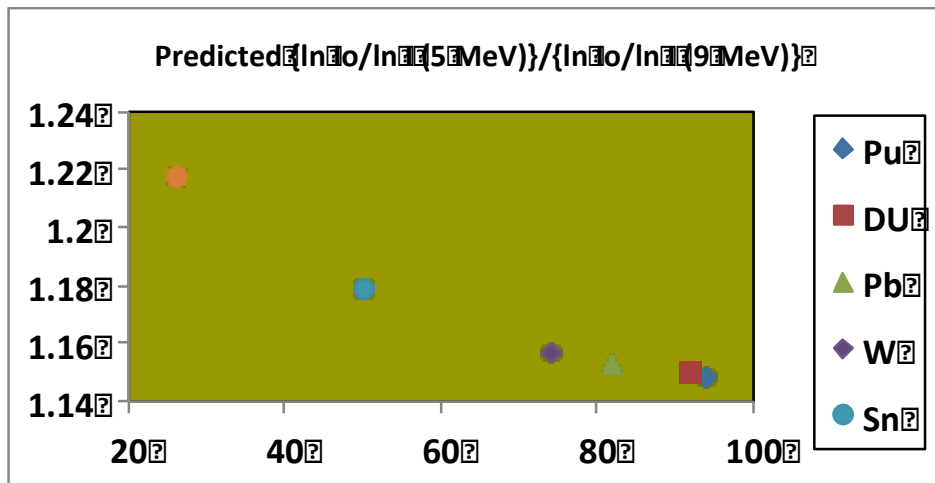


Figure 10. Predicted values of ratio values for the Set A data samples, measured axially.

Figure 11 (below) shows the ratio values of the Set B1 (4.64 cm) data samples, measured with the axis of the samples aligned with the x-ray beam (axial, or 0 degree). There is some evidence of clustering of the values for the higher Z elements, and the lower Z elements appear to follow a curve in the manner of the predicted results for Set A. The Set B1 data samples do not have equal areal density, so one should not expect the ratio values to fall along such a curve.

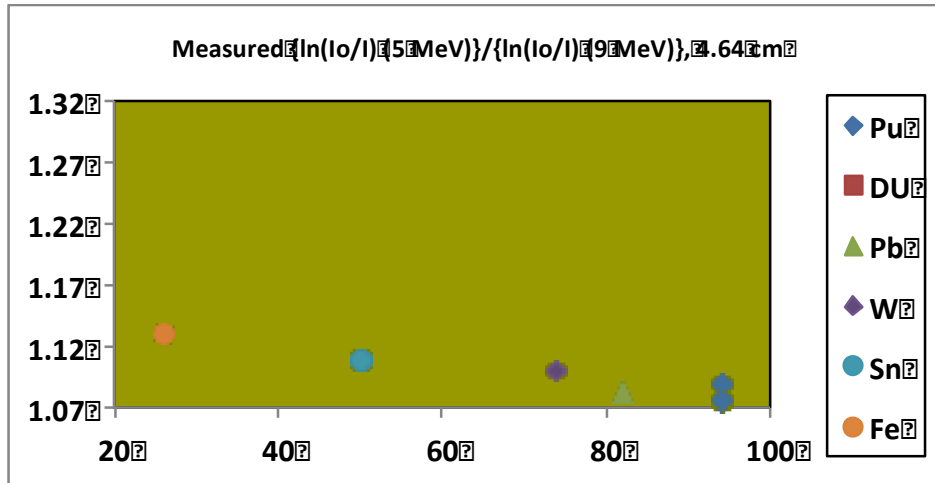


Figure 11. Measurements of ratio values for the Set B1 data samples, measured axially.

Figure 12 (below) shows the predicted ratio values of the Set B1 data samples, measured with the axis of the samples aligned with the x-ray beam (axial, or 0 degree). One could potentially set a threshold value for the ratio at approximately 1.22 based on the predicted results. However, the data acquired would indicate a different value for the threshold, and the failure of the results to behave as modeled would render any threshold meaningless.

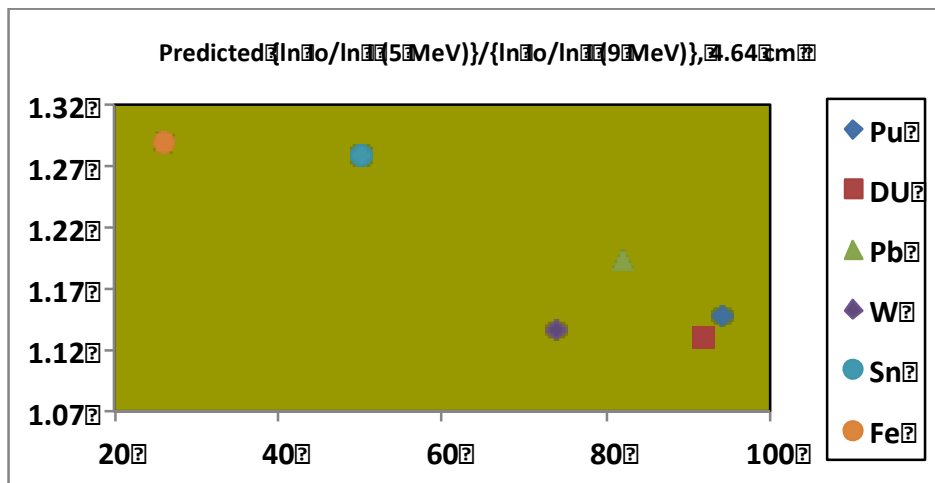


Figure 12. Predicted values of ratio values for the Set B1 data samples, measured axially.

### 6.3 Linear Detector Array Measurements

The measurements of the samples with the linear detector array are shown on the following figures. The measured results show the ratio values of the samples:

$$\ln(I_0/I)@5.4 \text{ MeV} / \ln(I_0/I)@9.6 \text{ MeV}$$

Error bars are calculated in accordance with the analysis procedure (Appendix A, section A.2.2).

Figure 13 (below) shows the ratio values of the Set A data samples, measured with the axis of the samples aligned with the x-ray beam (axial, or 0 degree). There is evidence of clustering of the values for the higher Z elements. The measurements of the lower Z elements skew to lower values for lower values of Z. One could set a threshold value for the ratio of approximately 1.08 based on the predicted results, and it would appear to apply well to the data acquired.

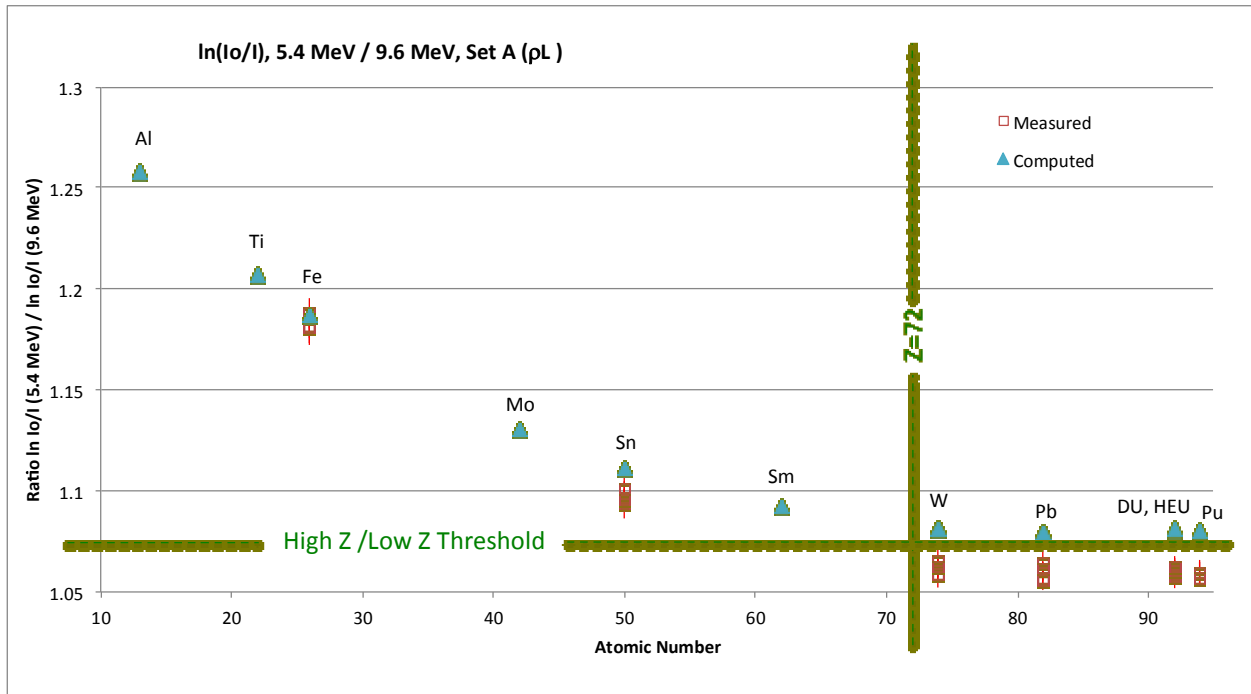


**Figure 13.** Ratio of material  $\mu\text{L}$  values of 5.4 and 9.6 MeV endpoint energy for a Linatron x-ray source, measured on Set A samples, oriented axially, Steel (Z=26), Tin (Z=50), Tungsten (Z=74), Lead (Z=82), DU (Z=92), HEU (Z=92) and WGPu (Z=94) on various dates, and computed (for Aluminum, Titanium, Steel, Molybdenum, Tin, Samarium, Tungsten, Lead, DU, HEU and WGPu; blue triangles). Dotted green lines denote  $Z \geq 72$  threshold for High-Z vs Low-Z materials (as defined by CAARS specification).

Figure 14 (below) shows the ratio values of the Set B1 (4.64 cm) data samples, measured with the axis of the samples aligned with the x-ray beam (axial, or 0 degree). There is evidence of clustering of the values for the higher Z elements. The measurements of the lower Z elements skew to lower values for lower values of Z. One could set a threshold value for the ratio of approximately 1.09 based on the data acquired. This higher threshold might result in false positives for Set A ( $\rho$ L) tin samples (see Figure 13). Alternatively, the use of a threshold of 1.08 (appropriate for the Set A ( $\rho$ L) samples) could yield a false negative for lead ( $Z=82$ ) as shown below.

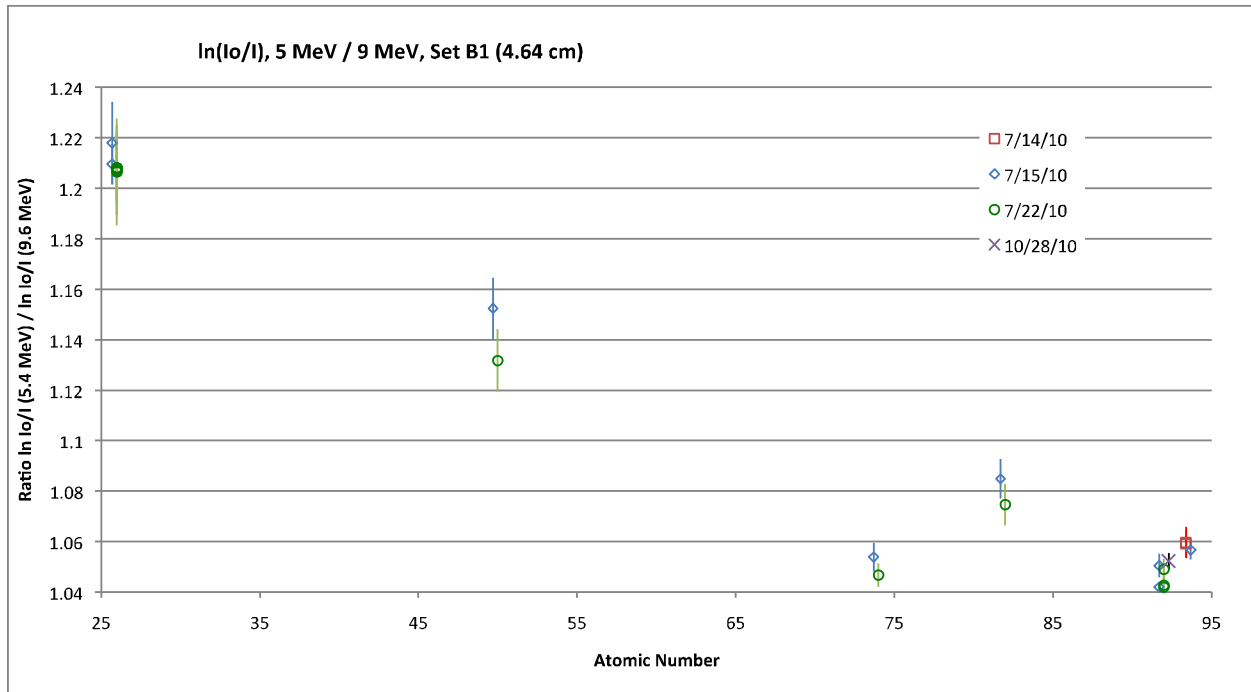
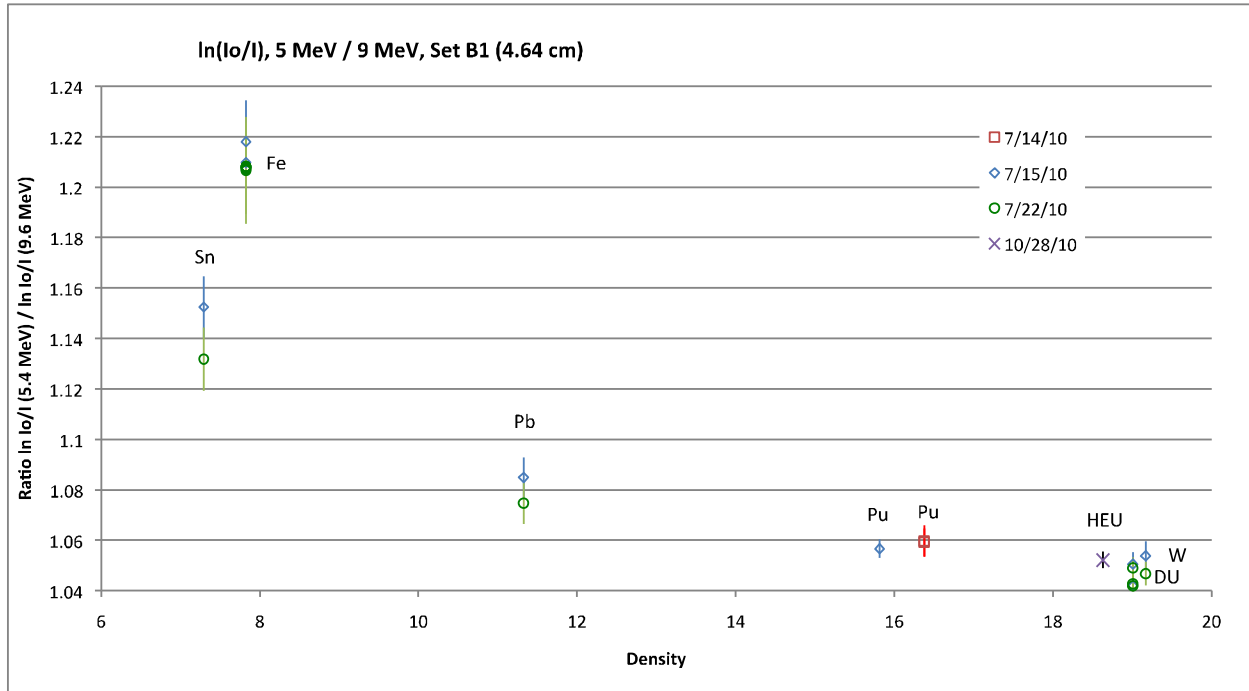


Figure 14. Measurements of ratio values for the Set A data samples, measured axially.

Figure 15 (below) shows the ratio values of the Set B1 (4.64 cm) data samples, measured with the axis of the samples aligned with the x-ray beam (axial, or 0 degree). In this graph the ratio (vertical axis) is plotted versus the density of the samples. There is evidence of clustering of the values for the higher density elements. One could set a threshold value for the ratio of approximately 1.09 based on the data acquired. This higher threshold might result in false positives for Set A ( $\rho$ L) tin samples (see Figure 13).



**Figure 15.** Measurements of ratio values for the Set A data samples, measured axially.

Figure 16 (below) shows the ratio values of the Set B2 (2.6 cm) data samples, measured with the axis of the samples normal with the x-ray beam (transverse, or 90 degree). There is evidence of clustering of the values for the higher Z elements. The measurements of the lower Z elements skew to lower values for lower values of Z. One could set a threshold value for the ratio of approximately 1.13 based on the data acquired. This higher threshold might result in false positives for multiple samples (see preceding figures).

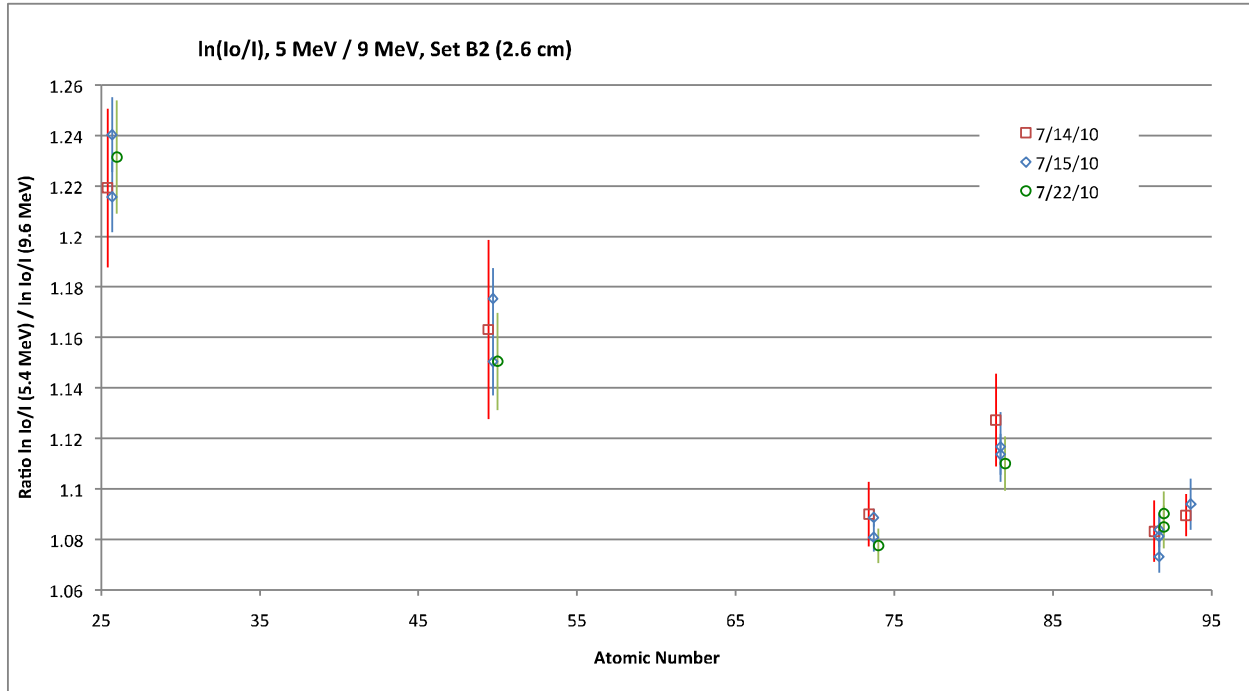


Figure 16. Measurements of ratio values for the Set B2 data samples, measured axially.

Figure 17 (below) shows the ratio values of the Set B2 (2.6 cm) data samples, measured with the axis of the samples normal with the x-ray beam (transverse, or 90 degree). In this graph the ratio (vertical axis) is plotted versus the density of the samples. There is evidence of clustering of the values for the higher density elements. One could set a threshold value for the ratio of approximately 1.13 based on the data acquired. This higher threshold might result in false positives for multiple samples (see preceding figures).

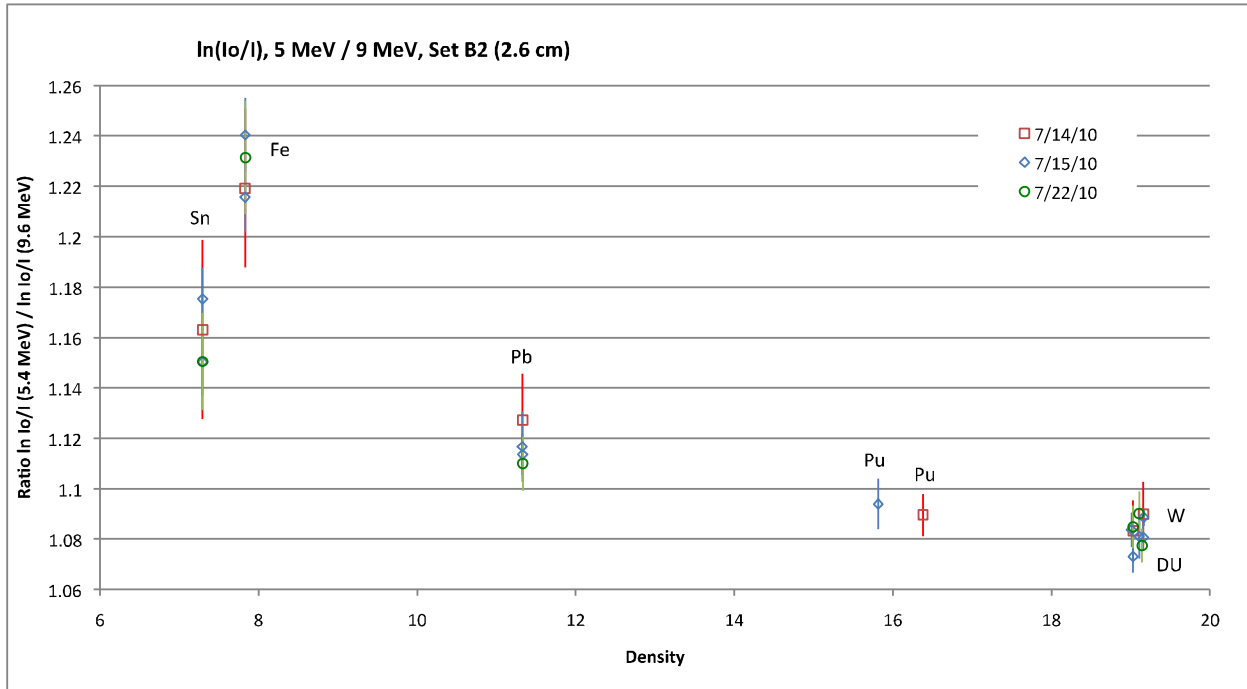


Figure 17. Measurements of ratio values for the Set B2 data samples, measured axially.

## 7. Conclusions

As expected, Depleted Uranium (DU) is a valid surrogate for Special Nuclear Materials (SNM) in CAARS ATD performance tests of transmission radiography systems. Transmission measurements of DU are nearly identical to SNM, and are distinct from lower Z materials. Use of DU as a surrogate for SNM will allow for valid field-testing of SNM detection systems, which utilize high-energy x-ray transmission measurement. This task included transmission measurements of DU and SNM with equipment that is nearly identical to current field systems.

The ratio of the x-ray linear attenuation coefficient times length ( $\mu L$ ) at 5.4 MeV, to  $\mu L$  at 9.6 MeV is a metric for atomic number (Z) based discrimination of materials. The measured ratios were compared with computed values based on LLNL photon cross section data and LLNL developed models of x-ray detector characteristics. Measured ratios for DU differed from HEU by an average of 0.25%, and from WGPU by 0.08%. For comparison, measured ratios for Sn differed from HEU by 3.2%, and from WGPU by 3.6%. Measured ratios for W differed from HEU by 0.01%, and from WGPU by 0.32%.

## **Appendix A          Detailed Test Procedures**

### ***A.1          Transmission Experiment Configuration***

#### *A.1.1      Equipment Required*

A Varian M9 dual-energy Linatron, Thales 14-bit amorphous silicon panel, 14" x 17", will be used in baseline imaging. A Varian linear array detector with pixel pitch 4.6 mm will also collect transmission data in detector studies.

#### *A.1.2      Physical Setup*

Transmission measurements will use collimation. Source-detector distance is approximately 6 meters.

#### *A.1.3      General Procedure*

Digital radiographs at 5.4 and 9.6 MeV will be acquired using a Varian M9 dual-energy Linatron. A typical test configuration is shown in A.3 (some of the dimensions were changed in actual practice). An initial set of measurements at 5.4 and 9.6 MeV will be taken with no target (i.e., no cans, holder or set of test objects) to characterize the beam profile. Imaging in the 90 degree direction gives an attenuation measurement for a standard thickness part. Frame averaging will be used to reduce noise and all data will be normalized by incident irradiance. In the case of the amorphous panel, 16 frames are acquired and averaged. For the linear detector array, 100 readouts are averaged. Thirty digital radiographs of each test will be acquired to perform adequate statistical analysis using the amorphous panel. Five measurement files will be acquired for linear detector array measurements.

### ***A.2          LDA transmission measurements***

#### *A.2.1      Data acquisition procedure for LDA transmission measurements*

Set up and prepare both the amorphous panel detector system and LDA system so they are prepped and ready to go. On the amorphous panel detector this means taking dark field images in raw (non-calibrated) format. On the LDA detector this means taking dark field images at both high energy and low energy settings. The settings differ in the number of source pulses to integrate the signal over: 8 for the high energy setting, 35 for the low energy setting. Each data acquisition includes 100 individual readouts of the array, 1 per group of pulses (either 8 or 35). Each acquisition of 100 readouts is written to a file. This is repeated five times, so that five files are generated for every measurement.

Use the gantry crane system to place the Linatron x-ray source in line with the Stonehedge II collimators and the amorphous panel. Set the Linatron collimator opening to four degrees horizontal opening and three degrees vertical opening.

Place the sample can, standing up with lid at top, on the rotary table in front of the amorphous panel. The Linatron laser spot should strike the can on axis, 85 mm above the bottom of the can. Adjust the height of the rotary stage if necessary.

The midstream collimators should be set to match the Stonehedge II openings. Set the source to “high” energy, and set the Varian detector to control the rep rate at 200 Hz by taking a dark field measurement in the high energy mode.

Turn on the x-ray source and take a series of panel images at 15 degree increments of the rotary table to establish the tilt, if any, of the sample in the can. For the non-SNM samples, open the can and correct any severe tilt of the sample. Repeat the series of images procedure if necessary. When completed, mark the can so that any remaining tilt and the position of the spider mount is readily apparent from the outside.

Remove the can from the rotary stage and move the source back to the linear detector array (LDA) position.

Close down the collimator to a fan (~2.8 degrees horizontal by ~0.1 degrees vertical, or about 1-2 mm). The vertical setting requires manual (local) control.

Move the sample stool into place in front of the source. Adjust the foam yoke pieces to properly center the sample in the beam path. Place the sample can in the yoke.

Take dark and air (source on) measurements on the LDA, at both high and low energy. Repeat each measurement five times.

Go back in and place the sample can on the stool. The measurement sequence is as follows:

- Dark measurement at high-energy settings with the source off.
- Sample measurement at high energy with the source on.
- Dark measurement at low-energy settings with the source off.
- Sample measurement at low energy with the source on.
- Dark measurement at high-energy settings with the source off.

Following the above sequence a different sample is placed on the stool, or the sample is positioned for a different orientation. Then the sequence is repeated.

Air measurements of the unattenuated source are interspersed with sample measurements throughout the day.

Once all measurements of the sample cans near the source (Mag~15) are completed, place the sample cans on the cart at the Mag =2 position for side-by-side axial measurements. Repeat the measurement sequence detailed above.

#### *A.2.2 Data analysis procedure for LDA transmission measurements*

ROI is chosen (individual detector channels selected).

For each measurement iteration the mean value of 100 repeats of selected channels is calculated (# of samples in mean = 100 x # of selected channels).

The mean value of the temporally adjacent dark image(s) is calculated for the selected channels over 100 readouts.

Mean value is calculated for five repeats of measurement of sample with the source on.

A dark adjusted value is calculated for each of the five mean values.

The mean of the five adjusted means is calculated, as is the std dev of the five adjusted means.

The ratio of the std dev of the mean of means, to the mean of means, is calculated for the group of five repeats of the measurement.

The process is repeated for the light field measurements of the same detector channels.

The adjusted light field mean is divided by the adjusted signal mean to yield a value of  $I_o/I$ .

The std dev / mean ratios for the light and signal are added in quadrature (square root of the sum of the squares).

The quadrature value is multiplied by  $I_o/I$  to yield a relative uncertainty of  $I_o/I$ .

The relative uncertainty of  $I_o/I$  is both added to and subtracted from  $I_o/I$  to yield high and low range values.

Natural logs are calculated on  $I_o/I$  as well as the high and low range values for  $I_o/I$ .

The natural log of the low range  $I_o/I$  is subtracted from the natural log of the high range  $I_o/I$ , divided in half, and divided by  $\ln(I_o/I)$  to yield the relative uncertainty in  $\ln(I_o/I)$ .

The foregoing calculations are repeated for high (9.6 MeV endpoint) and low (5.4 MeV endpoint) energy measurements.

The  $\ln(I_o/I)$  at 5.4 MeV is divided by the  $\ln(I_o/I)$  at 9.6 MeV to arrive at the ratio of logs value for the material that was measured.

The relative uncertainties of  $\ln(I_o/I)$  calculated at the two energies are added in quadrature and multiplied by the ratio of logs to arrive at the uncertainty in the measurement of the ratio of logs.

This last value is added and subtracted from the ratio of logs and shown on the graphs as the error bars for the ratio of logs values.

### ***A.3 Archive: Test Plan for Amorphous panel transmission measurements***

#### CAARS Task 2 – Proposed Revisions to Test Plan

10/1/09

Task 2.1: Sample sets – 2 sets, Set A and Set B

##### Set A

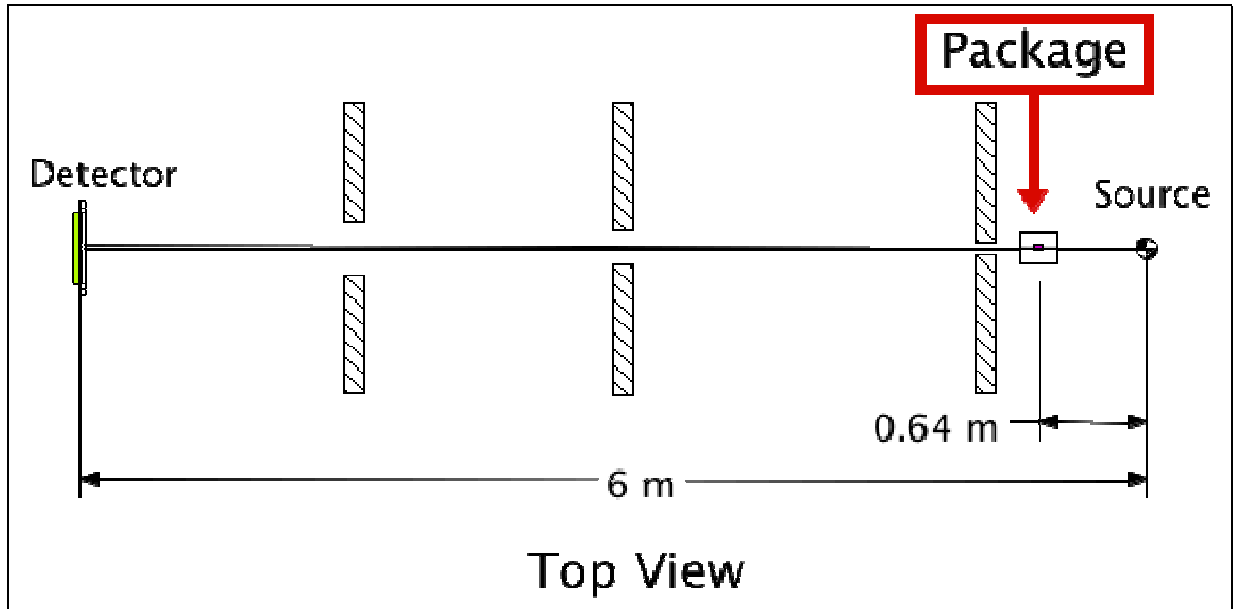
- The quantity (density x length) is equal for all samples
- Samples equivalent to existing samples Pu-1, Pu-2  
 $\rho x = 73.4 \text{ g/cm}^2$
- 7 materials, 3 samples each, diameter = 2.6 cm  
WGPu, HEU, DU, Pb, W, Sn, Fe
- All samples monolithic (1 piece) except HEU (2 pieces)

##### Set B

- The length is 4.64 cm for all samples  
Length based on side of  $100 \text{ cm}^2$  cube (= 4.64 cm)
- 7 materials, 1 sample each, diameter = 2.6 cm  
WGPu, HEU, DU, Pb, W, Sn, Fe
- All samples monolithic (1 piece) except HEU (2 or 3 pieces), Pb, W and DU (2 pieces each)

### Task 2.2: Transmission Measurements

Perform transmission measurements to minimize effect of scattering by test sample.



#### General measurement characteristics

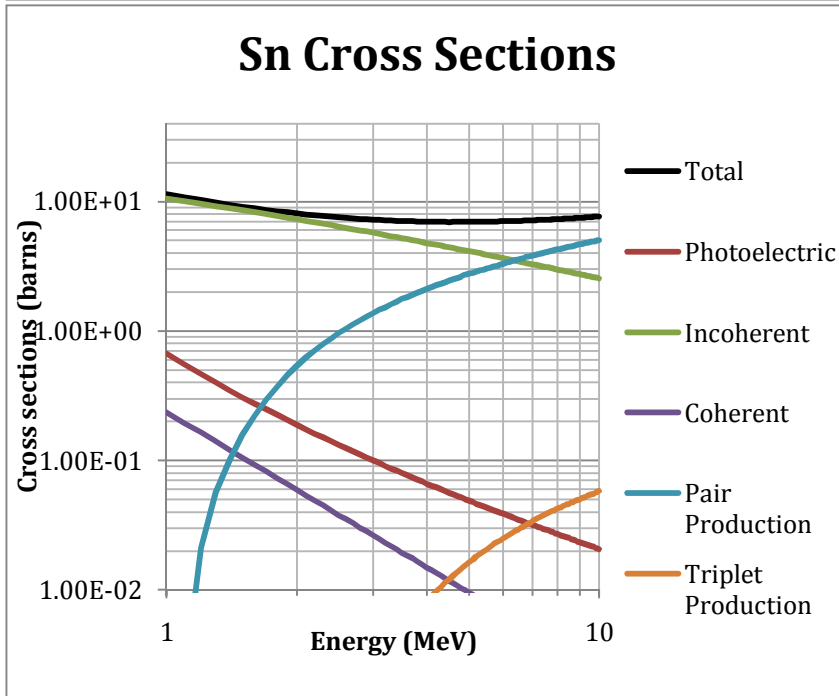
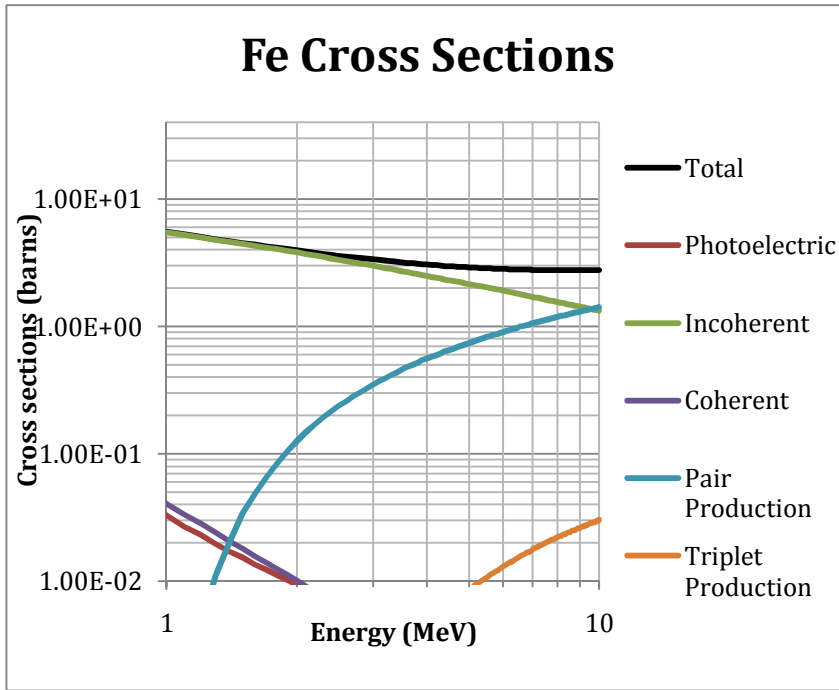
- One sample per DR image
- Highly collimated beam
- Statistical data collection – 30 images of each sample
- 9 MeV (nominal, 9.6 MeV calculated) linear accelerator x-ray source
- Amorphous silicon detector panel, normalized and bad pixel corrected
- Sample rods are packaged in 1 gal paint can, held in place along the axis of the can by a spider mount, in turn held in place by foam doughnuts
- Sample packages are imaged near detector to verify placement of sample along central axis of package can, and to place outside markings indicating sample location
- 0° and 90° images taken on all samples
- 0° measurements are taken with beam aligned with center of sample rod, along rod axis
- 90° measurements are taken with beam perpendicular to the rod axis, near the center of the rod length, or in the case of multi segment rods, near the center of the longest segment
- Sample package cans rest in foam yokes to ensure samples are in the same, repeatable location for each measurement
- Dark (no X rays) and light (X rays on, no sample present) measurements taken at beginning of day and periodically throughout
- Steel and DU samples periodically measured for tracking any systemic drift

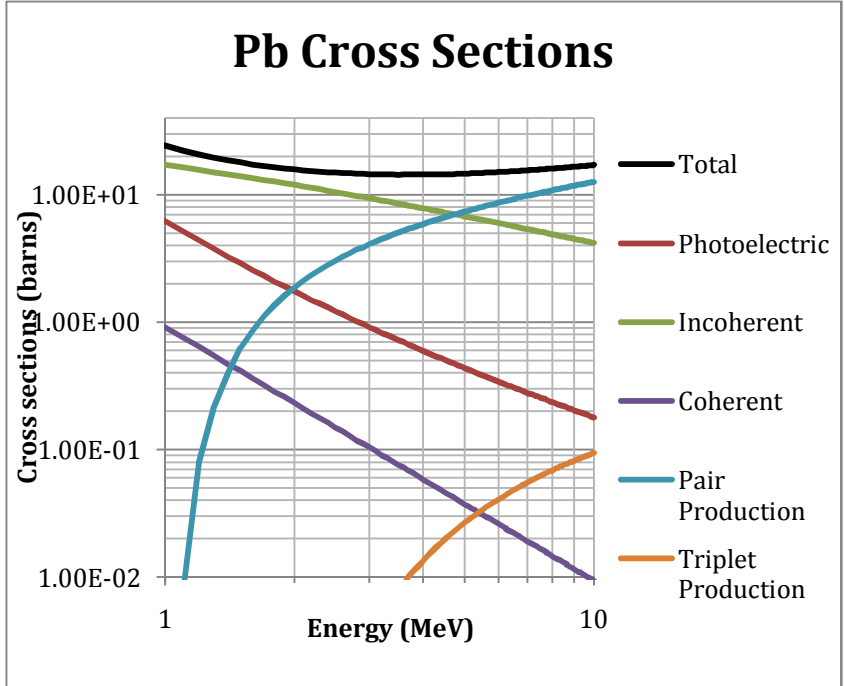
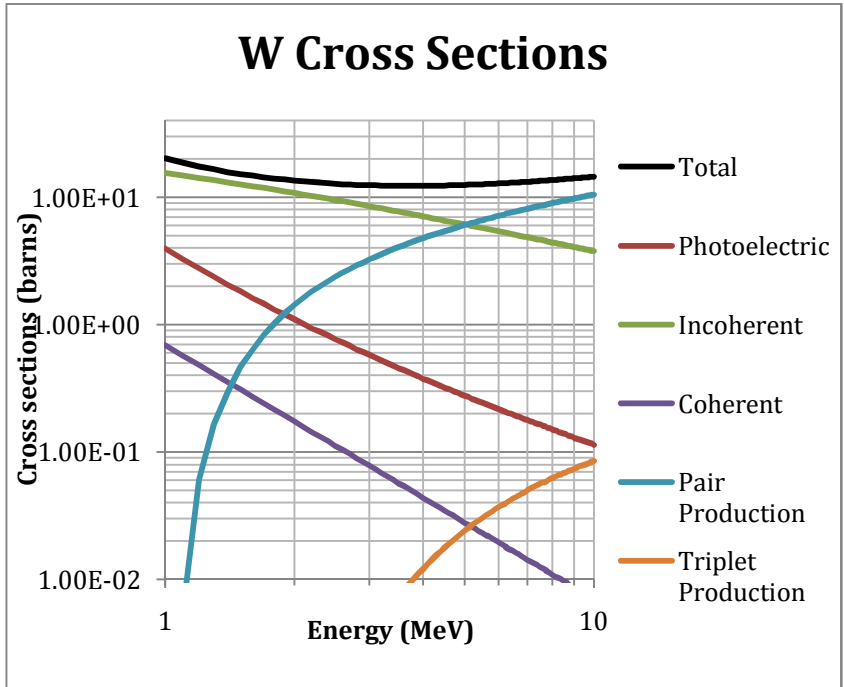
- Each sample measurement is composed of 16 individually acquired frames which are averaged together, output as a single image file

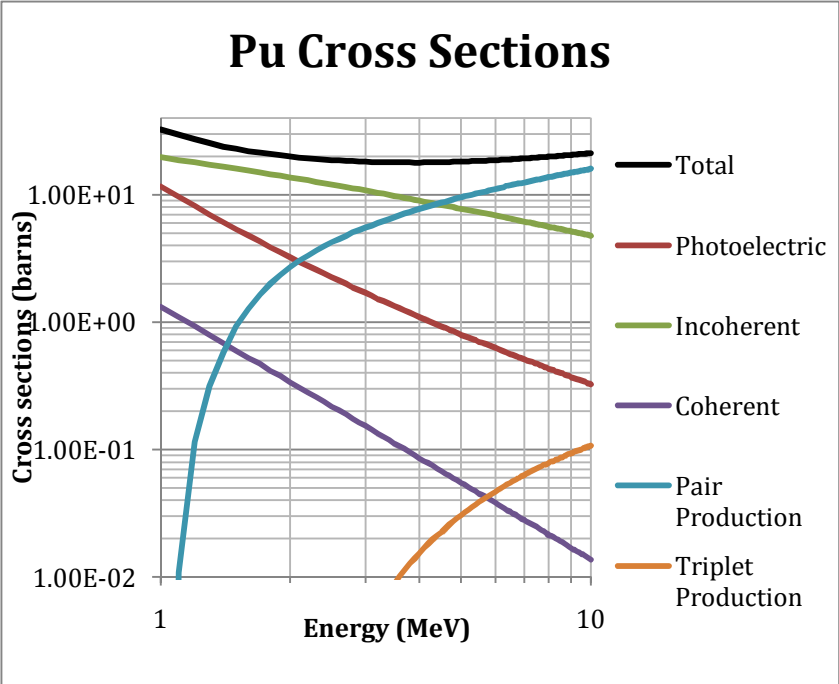
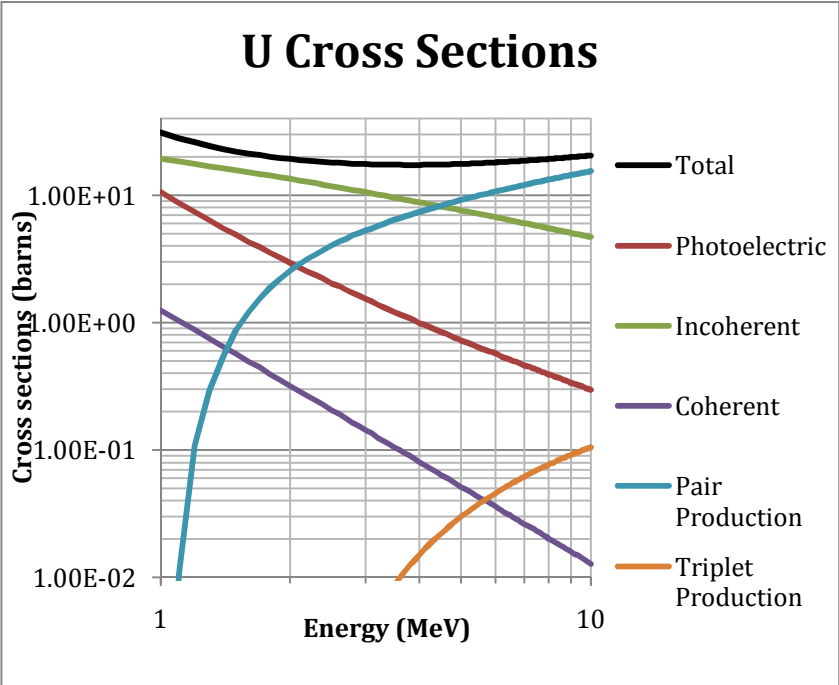
Specific measurement procedures for each sample can

- Check x-ray source alignment, output and collimation ( $\sim 0.5^\circ$  opening, vertical and horizontal)
- Check that detector panel settings and software calibration files are in agreement
- Set detector frame count to 1
- Record x and y coordinates of center of collimated x-ray beam at panel
- Increase opening of x-ray source collimation ( $\sim 3^\circ$  vertical opening,  $\sim 4^\circ$  horizontal)
- Sample packaging verification:
  1. Place sample can on rotary stage, near detector panel, with axis of can aligned with rotary stage axis
  2. Mark outside of sample can at 85 mm from can bottom rim to indicate approximate center of sample rod
  3. Use x-ray source alignment laser and a radiograph to verify position of sample rod within sample can
  4. Radiograph sample can at two orthogonal rotations to verify that sample rod is coaxial with sample paint can
    - a. For SNM samples, mark outside of sample can to indicate tilt of sample axis relative to sample can axis
    - b. For non-SNM samples, adjust sample position within can as needed
  5. Set stage position so that x-ray beam is aligned with two of the plates of the sample can internal spider mount apparatus
  6. Mark outside of sample can with permanent marker to indicate position of internal spider mount apparatus
- Install apparatus for positioning sample cans near x-ray source head (stool, stand, yoke, shim materials)
- Place sample near source, with the can axis horizontal, and radiograph at  $90^\circ$  to verify sample orientation
- Shim yoke supports as needed to make sample rod horizontal
- Place sample at  $0^\circ$  and radiograph
- Shim yoke supports and adjust sample can position as needed to make sample rod coaxial with  $0.5^\circ$  collimation
- Set detector frame count to 16
- Acquire 30 radiographs of sample at  $0^\circ$  orientation
- Place sample at  $90^\circ$  orientation and acquire 30 radiographs

## Appendix B Photon Cross Sections







**Appendix C                      Acronym List and Glossary**

**– A –**

- A                      Mass Number
- Al                     Aluminum
- ATD                  Advanced Technology Demonstration

**– B –**

bremsstrahlung        The term literally means "braking radiation". When a speeding electron encounters the nucleus of an atom it will slow down and in this process photon radiation (i.e. x-rays) is produced.

**– C –**

CAARS                 Cargo Advanced Automated Radiography System

Category III materials        a term applied to special nuclear materials (SNM). Category I/II quantities of SNM are determined by grouping materials by type, attractiveness, and quantity. Category I/II require the highest security. Lesser amounts of material are graded as Category III or IV and have reduced security requirements.

Compton electron        An electron that has encountered an energetic photon and caused Compton scattering; as a result the struck electron then also acquires energy and begins to energetically move through a material.

Compton scattering        The process by which an energetic photon - as it moves through a material - encounters an electron in an atom and changes direction.

**– D –**

- DHS                    U.S. Department of Homeland Security
- DNDO                 Domestic Nuclear Detection Office
- DR                     Digital Radiography
- DU                     Depleted Uranium

– E –

– F –

Fe Iron

FSP facility safety plan; a guidance document that prescribes precautionary standards for working with potentially hazardous materials or under potentially hazardous conditions.

– G –

– H –

HEU Highly Enriched Uranium

– I –

incoherent scattering an x-ray that has scattered from an electron and changed some of its wave-like properties; see Compton scattering

– J –

– K –

k Thousand

– L –

L-3 L-3 Communications

LDA Linear Detector Array

LLNL Lawrence Livermore National Laboratory

– M –

MCNP Monte Carlo N-particle Transport Code, a computer code that uses a statistical technique to determine the effect that a medium has on a photon or particle as it passes through it.

MeV Million Electron Volts

Mo Molybdenum

– N –

nuclear

resonance  
fluorescence

selective absorption and re-emission of photon radiation from an atom. This phenomena forms the basis of a sensitive analytic technique for measuring the presence of atomic or molecular species.

– O –

– P –

pair production

a phenomena that occurs when a high energy photon interacts with the electromagnetic field of an atom. In this process an electron-positron pair is created and the energy of the photon is reduced by an amount equal to the mass rest mass and kinetic energy(1.022 MeV) of the two new particles. Photons with energies less than 1.022 MeV cannot cause pair production

Pb

Lead

Pu

Plutonium

– Q –

– R –

– S –

Sn

Tin

Sm

Samarium

SNM

Special Nuclear Material

Stonehenge

Whimsical reference to the array of collimators forward of the x-ray generator used in the present studies; these help focus the beam on the target

– T –

Ti

Titanium

– U –

U.S.

United States

– V –

– **W** –

Varian Linatron      Brand name of a device that is used to make high-energy x-rays for experimental studies described in the present document.

W                      Tungsten

WGPu                Weapons Grade Plutonium

– **X** –

– **Y** –

– **Z** –

Z                      Atomic Number